

One-step synthesis of Mn_3O_4 nanoparticles: Structural and magnetic study

América Vázquez-Olmos^{a,*}, Rocío Redón^a, Geonel Rodríguez-Gattorno^b,
M. Esther Mata-Zamora^a, Francisco Morales-Leal^c, Ana L. Fernández-Osorio^d,
José M. Saniger^a

^a Centro de Ciencias Aplicadas y Desarrollo Tecnológico, México, DF 04510, Mexico

^b Instituto de Física, México, DF 04510, Mexico

^c Instituto de Investigación en Materiales, México, DF 04510, Mexico

^d Facultad de Estudios Superiores, Cuautitlán-1, Universidad Nacional Autónoma de México, Coyoacán, México, DF 04510, Mexico

Received 16 February 2005; accepted 2 May 2005

Available online 6 July 2005

Abstract

One-step room-temperature synthesis of nanocrystalline Mn_3O_4 hausmannite, without heating posttreatment, was carried out from a simple dissolution of manganese(II) acetate in a mixture of *N,N'*-dimethylformamide (DMF) and water. Homogeneous nanocrystals like rods were obtained, with an average width and length of 6.6 ± 1.2 nm and 17.4 ± 4.1 nm, respectively, and a preferential growth along the (001) direction. Magnetization measurements on a powdered sample showed ferrimagnetic behavior at low temperatures. Under zero-field cooling (ZFC) measurement at 100 Oe, the observed blocking temperature (T_B) was 37 K.

© 2005 Elsevier Inc. All rights reserved.

Keywords: Nanoparticles; Hausmannite; Colloidal dispersion; Magnetic materials

1. Introduction

Manganese oxides are materials with a wide range of applications, such as batteries, catalysts, and electrochromic and magnetic materials [1–3]. In particular, Mn_3O_4 is known to be an effective and inexpensive catalyst to limit the emission of NO_x and CO, which provides a powerful method of controlling air pollution. This material has also attracted interest as an active catalyst for the reduction of nitrobenzene or oxidation of methane. It has been shown to be a corrosion-inhibiting pigment for epoxy–polyamide and epoxy–ester based primers and top coating [1,3,4]. Moreover, Mn_3O_4 has been used as one of the raw materials in the manufacture of soft magnetic materials such as manganese zinc ferrite, which is useful for magnetic cores in transformers for power

supplies [5–7]. Nanometer-sized Mn_3O_4 , with notable increased surface area and greatly reduced size, is expected to display better performance in these aspects of application.

Manganese oxides crystallize in several different structures with varied proportions of Mn in different oxidation states (+2, +3 and +4) [8]. Mn_3O_4 is an oxide with the normal spinel structure. The stable room-temperature phase is tetragonal hausmannite (space group $I4_1/amd$) with Mn^{3+} and Mn^{2+} ions occupying the octahedral and tetrahedral positions of the spinel structure, respectively. The octahedral symmetry is tetragonally distorted due to the Jahn–Teller effect on Mn^{3+} ions [9]. Mn_3O_4 is a model spinel compound for many experimental and theoretical investigations; however, the majority of these are related to the bulk material [8–13].

Usually, when heated to about 1000 °C in air, all oxides, hydroxides, carbonates, nitrates, and sulfates of manganese can form Mn_3O_4 . In addition, it has also been re-

* Corresponding author. Fax: +52 55 5622 8651.

E-mail address: amer@aleph.cinstrum.unam.mx (A. Vázquez-Olmos).

ported that precipitated manganese dioxide can be reduced to Mn_3O_4 under a hydrogen atmosphere at 200 °C [3]. Furthermore, in the last decade, solution chemical synthesis techniques such as the sol–gel process and the solvothermal method have been employed to prepare hausmannite; however, these processes still require posttreatment at different temperatures [14]. Recently, Qian and co-workers [15] reported a one-step low-temperature (140 °C) synthesis of Mn_3O_4 nanorods in alcohol–water mixtures, using KMnO_3 as a starting manganese source and Na_2SO_3 as a reducing agent.

On the other hand, DMF and dimethyl sulfoxide (DMSO) have been proved to be very useful solvents in nanoparticle synthesis [16–21]. Their high dielectric constants allow charge separation, turning them into good solvents for ionic solids and polar or polarizable molecules.

Thus, herein we present a facile one-step process for the preparation of nanocrystalline Mn_3O_4 from $\text{Mn}(\text{OAc})_2 \cdot 4\text{H}_2\text{O}$ in DMF– H_2O (10%) at room temperature and its spectroscopic, structural, and magnetic study. The present contribution constitutes a very important advance in nanostructure Mn_3O_4 preparations, especially for those applications that require clean nanostructured materials.

2. Experimental

2.1. Materials

Manganese acetate tetrahydrate, $\text{Mn}(\text{OAc})_2 \cdot 4\text{H}_2\text{O}$ (99% Aldrich), *N,N'*-dimethylformamide, DMF (99.8% Aldrich), and acetone, $\text{CO}(\text{CH}_3)_2$ (Fermont 99.7%), were purchased and used as received, without further purification. Ultrapure water (18 M Ω /cm) was obtained from a Barnsted E-pure deionization system.

2.2. Synthesis

A quantity of 0.03063 g of $\text{Mn}(\text{OAc})_2 \cdot 4\text{H}_2\text{O}$, was dissolved in DMF (22.5 ml) under vigorous stirring. After this, 2.5 ml of ultrapure water was added for the synthesis of colloidal Mn_3O_4 nanorods to get a final concentration of 5×10^{-3} M in 25 ml of DMF– H_2O (10%). The amber solution was stirred for a further 30 min and the resulting solution left to stand for 3 months to yield a dark brown precipitate, which was separated by centrifugation (16,000 rpm \times 10 min) and washed with acetone.

2.3. Instruments

UV–visible absorption spectra, in colloidal dispersion and powder, were determined on an Ocean Optics USB2000 miniature fiber optic spectrometer. The Fourier transformed infrared (FTIR) spectroscopy was done in a Nicolet Nexus 670 FT-IR infrared spectrometer from 4000 to 400 cm^{-1} with a resolution of 4 cm^{-1} , on a KBr wafer. The X-ray

diffraction pattern was measured in D5000 Siemens equipment using $\text{CuK}\alpha$ radiation ($\lambda = 1.5406 \text{ \AA}$). Transmission electron microphotographs (TEM) were obtained in a JEOL 1200EXII instrument, operating at 60 kV, by deposition of a drop of the colloidal dispersion of Mn_3O_4 onto 200 mesh Cu grids coated with a carbon/collodion layer. High-resolution transmission electron microphotographs (HR-TEM) were obtained in a JEOL 2000F instrument, operating at 200 kV, using the same sample preparation as in TEM. The particle size distribution was determined from digitalized amplified micrographs by averaging the larger and smaller axis diameter measured in each particle. Morphology calculations of Mn_3O_4 crystal were done by the program SHAPE v7.1.2 (free demo from www.shapesoftware.com) based on simple geometric considerations according to Bravais–Friedel–Donnay–Harker (BFDH) methodology [22–24].

Magnetic measurements were performed on a SQUID Quantum Design magnetometer on powdered samples of Mn_3O_4 nanoparticles. The temperature was varied between 2 and 300 K according to zero-field-cooling (ZFC)/field-cooling (FC) procedure at 100 Oe, and the hysteresis loop was obtained at 5 K in a magnetic field of up to ± 3 T.

3. Results and discussion

3.1. Spectroscopic study

The colloidal dispersion of Mn_3O_4 was monitored by UV–visible electronic absorption spectroscopy, as shown in Fig. 1. At the beginning the UV–visible spectrum of a freshly prepared solution of $\text{Mn}(\text{OAc})_2 \cdot 4\text{H}_2\text{O}$ in DMF– H_2O (10%), exhibits a wide absorption band with an onset at 440 nm (Fig. 1b); 1 week later, this band becomes wider and the onset shifts to 558 nm (Fig. 1c). The spectrum remains unchanged after 3 months, when the Mn_3O_4 precipitates as a brown fine powder. The electronic absorption spectrum of the precipitate obtained by diffuse reflectance measurement (Fig. 1d) shows three well-defined regions, one going from 250 to 410 nm, another from 410 to 585 nm, and the last one finishing at 810 nm. The first portion is attributed to the allowed $\text{O}^{2-} \rightarrow \text{Mn}^{2+}$ and $\text{O}^{2-} \rightarrow \text{Mn}^{3+}$ charge transfer transitions, and the last two can be reasonably related to d–d crystal field transitions, ${}^3\text{E}_g(\text{G}) \leftarrow {}^3\text{T}_{1g}$, ${}^3\text{A}_{2g}(\text{F}) \leftarrow {}^3\text{T}_{1g}$, ${}^3\text{A}_{2g}(\text{G}) \leftarrow {}^3\text{T}_{1g}$, ${}^3\text{T}_{2g}(\text{H}) \leftarrow {}^3\text{T}_{1g}$, ${}^3\text{T}_{1g}(\text{H}) \leftarrow {}^3\text{T}_{1g}$, and ${}^3\text{E}_g(\text{H}) \leftarrow {}^3\text{T}_{1g}$, on octahedral Mn^{3+} species. This spectrum is similar to the one reported by Boyero et al. for the hausmannite phase [11].

The precipitate was analyzed by FTIR spectroscopy from 4000 to 400 cm^{-1} . The spectrum (Fig. 2) shows the characteristic absorption bands of $\nu\text{Mn–O}$ vibrations at 639, 532, and 409 cm^{-1} , together with a weak band at 1046 cm^{-1} , which can be attributed to $\nu\text{Mn–O–H}$ vibration. Finally, a broad band at 3423 and an other weak band at 1630 cm^{-1} were observed due to absorbed water. This FTIR spec-

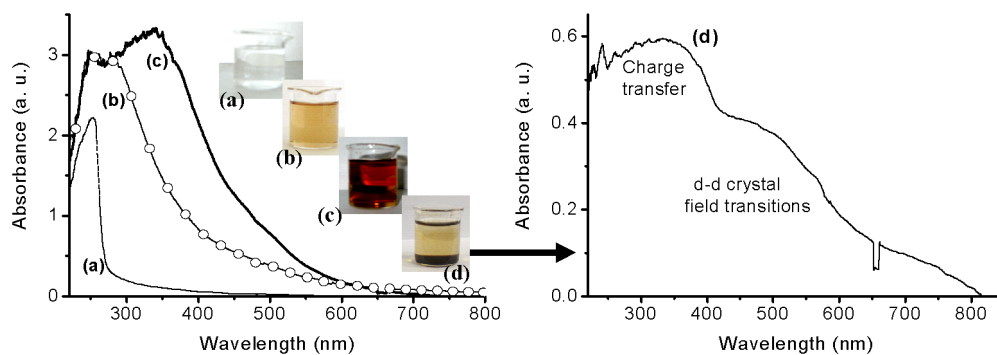


Fig. 1. Left: UV-visible electronic absorption spectra of (a) solvent mixture of DMF and H₂O (10%), (b) Mn(OAc)₂·4H₂O 5×10^{-3} M immediately after dissolving and (c) 1 wk later. This spectrum remains unchanged after 3 months, when Mn₃O₄ hausmannite precipitates as brown powder. Right: (d) absorption spectrum of the powder sample.

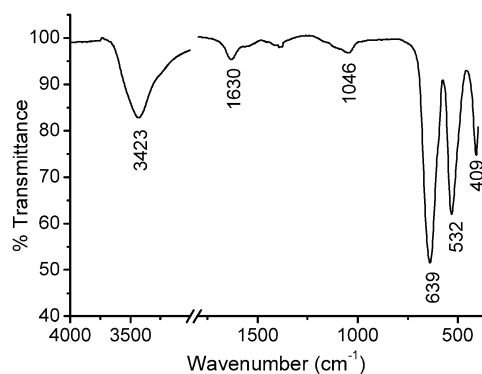


Fig. 2. FTIR spectrum of a Mn₃O₄ nanorod powdered sample.

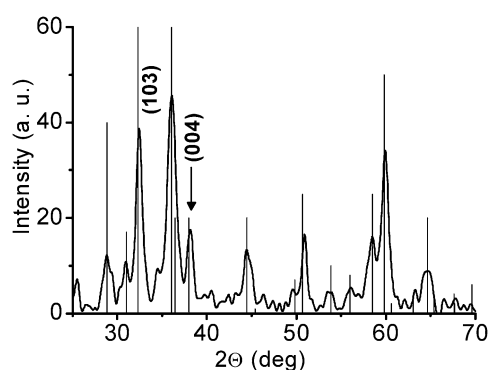


Fig. 3. XRD pattern of Mn₃O₄ nanoparticles. The peaks marked were used to determine the average crystallite size. All peaks can be indexed to Mn₃O₄ hausmannite, JCPDS No. 24-0734.

trum was consistent with reported references for Mn₃O₄ [3,11,12].

3.2. Structural study

The X-ray powder diffraction pattern (Fig. 3) reveals the formation of a nanocrystalline product consistent with the spinel structure of Mn₃O₄. All diffraction peaks can be perfectly indexed to the hausmannite structure (JCPDS Card 24-0734). The average crystallite size of 20.9 ± 0.19 nm was calculated from the peak broadening method, using the

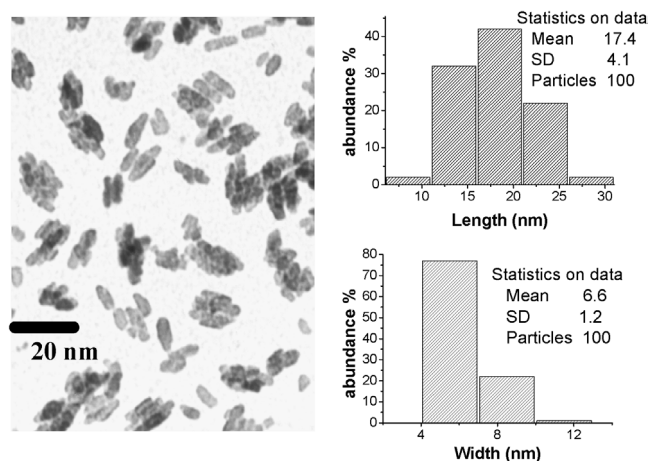


Fig. 4. TEM micrograph of Mn₃O₄ nanorods and the particle size distribution histograms.

classical Scherrer–Warren equation over the (004) and (103) reflection. The relative intensity for the {001} reflections is twice the size of the reported values, which reveals a preferential orientation of nanocrystals along the (001) direction.

On the other hand, TEM micrograph obtained from an Mn₃O₄ colloidal dispersion sample (after two weeks of its synthesis) allowed us to confirm preferential growth of the Mn₃O₄ nanostructures (Fig. 4). The particle size distribution was determined over 100 nanorods, being average width and length of 6.5 ± 1.2 nm and 17.4 ± 4.1 nm, respectively. The average particle size obtained from the XRD pattern is in agreement with the average length value observed.

HRTEM micrographs also corroborate the presence of elongated nanocrystals with dimensions close to those determined by X-ray and TEM experiments. In Fig. 5, a representative single elongated nanocrystal with a dimension of 8.3×19.3 nm, can be observed; the interplanar spacing of 2.89 Å corresponds to the (200) plane of tetragonal Mn₃O₄. In addition, the electron diffraction pattern confirms the nanorods to be composed of Mn₃O₄.

Qian and co-workers [15] reported their prepared nanorods to be oriented perpendicular to the normal direction of (101) lattice planes, this being one of the natural grow-

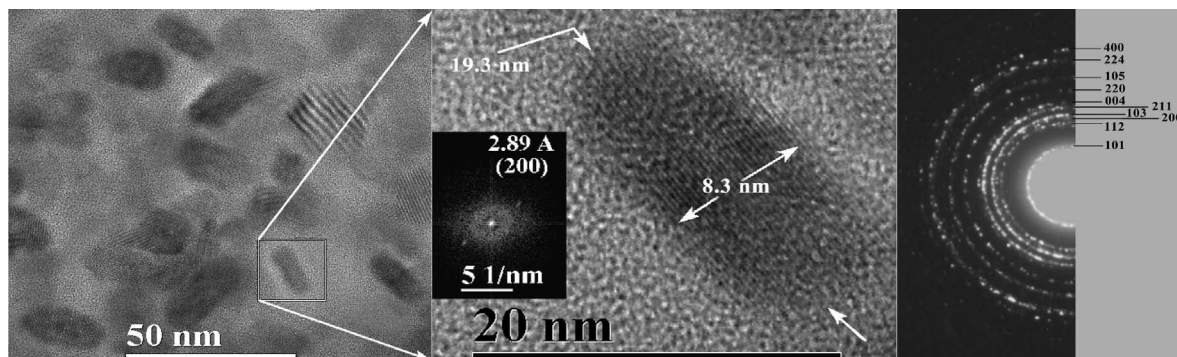


Fig. 5. HR-TEM micrographs of the Mn_3O_4 nanorods. Right, the corresponding electron diffraction pattern.

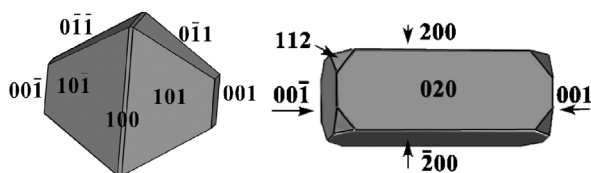


Fig. 6. Expected crystal habits for Mn_3O_4 according to Bravais–Friedel–Donnay–Harker method, calculated with SHAPE software, version 7.1.2.

ing directions expected for hausmannite. However, in the present case it is noteworthy that the rods are oriented with an axial direction parallel to the $\langle 001 \rangle$ zone axis. Tetragonal Mn_3O_4 is expected to crystallize in a crystal habit as shown in Fig. 6 (left); depending on the synthesis conditions, $\langle 001 \rangle$ faces can appear with more or less importance [25]. Fig. 6 (right) shows the calculated morphology for one Mn_3O_4 crystal, obtained with the SHAPE v7.1.2 program. In the latter case, the calculated crystal habit was done assuming a favored growth along the $\langle 001 \rangle$ direction. In this case the morphology matches exactly with the experimental results.

A possible explanation regarding the morphology of Mn_3O_4 nanoparticles obtained under the present reaction conditions may be that the growth of the $\{101\}$ nanocrystals plane faces depends on the availability of Mn^{3+} , which in turn depends on the oxidation of Mn^{2+} (the oxidation process will be discussed later). The growth along the $\langle 001 \rangle$ direction seems to be favored by the fact that the density of Mn^{3+} in the $\langle 001 \rangle$ faces is lower than that in the natural expected growing direction (e.g. $\langle 110 \rangle$) (Fig. 7).

3.3. Magnetic study

In bulk and monocrystal, Mn_3O_4 hausmannite is ferrimagnetic, with a Curie temperature of about 42 K [26–28]; the Mn_3O_4 nanorod sample also has ferrimagnetic behavior at low temperatures, being paramagnetic at room temperature. ZFC measurement was carried out, cooling from room temperature to 2 K without any external magnetic field. Then a magnetic field of 100 Oe was applied, and the magnetization of the sample was measured following the rise of

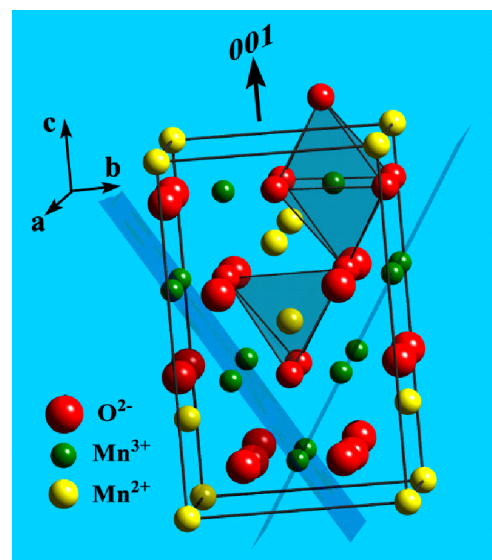


Fig. 7. Crystal model of Mn_3O_4 , the highlighted planes indicate the direction where the Mn^{3+} concentration is higher.

the temperature. When the temperature approaches 37 K, the magnetization reaches a maximum and then starts to decrease. The temperature at which the thermal activation overcomes all the energy barriers is known as the blocking temperature, T_B [29,30] (Fig. 8). This result is similar to that reported by Park and co-workers [14] for Mn_3O_4 spherical nanoparticles of 6 nm. Moreover, in the FC measurement, the sample was initially cooled to 2 K under an applied magnetic field of 100 Oe. The subsequent magnetization measurement was recorded from 2 to 300 K with the magnetic field kept at 100 Oe, a transition temperature ≈ 40 K being observed.

Although the hysteresis loop was obtained at 5 K in a magnetic field of up to ± 30 kOe (Fig. 8), the saturation magnetization (M_s) was not reached, showing a maximum of magnetization (M_{\max}) at about 26 emu/g; this value represents 68.4% of the saturation magnetization in the bulk ($M_s \text{ Mn}_3\text{O}_4 = 38$ emu/g) [31]. A remanence ratio (M_r/M_{\max}) of 0.77 was estimated from the remanence value (M_r) of 20 emu/g. The coercivity (H_c) for these nanorods was of 5.2 kOe.

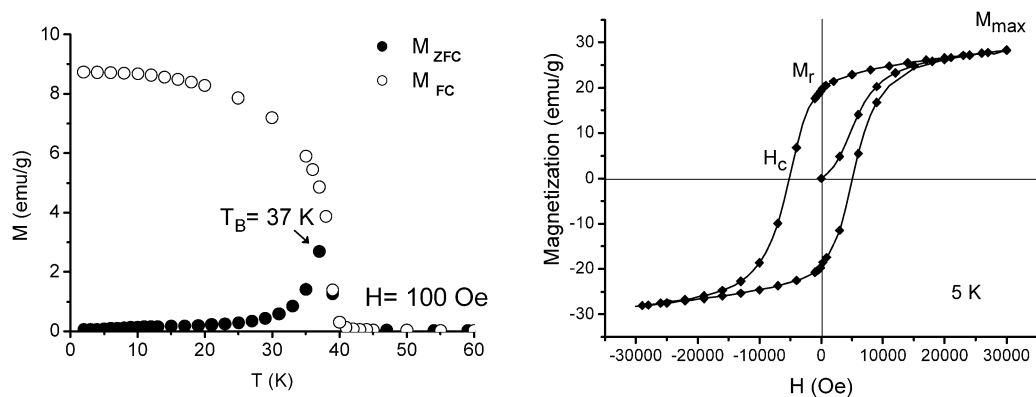


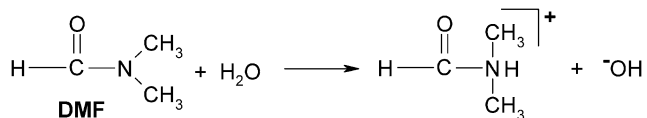
Fig. 8. Zero-field-cooled (ZFC) and field-cooled (FC) magnetization curves of Mn_3O_4 nanorods under an applied field of 100 Oe (left). Hysteresis loop at 5 K (right).

As expected, the magnetic behavior is under the influence of rod size. A principal effect of finite size is the breaking of a large number of bonds on the surface cations, producing a core of aligned spins surrounded by a disordered shell. This can result in a disordered spin configuration near to the surface and a reduced average net moment compared to the bulk materials. In addition, the surface spin states can result in high field hysteresis and relaxation of the magnetization [32], as has been observed for these nanorods.

3.4. Proposed reaction scheme

In general, the obtaining of metal oxides requires a basic medium, and usually NaOH or LiOH [25] is employed for this purpose.

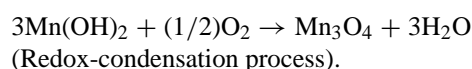
However, in this work, the solvent mixture generates the basic medium, due to a hydrolysis mechanism, turning the solvents into a good source of hydroxyl anions [18]:



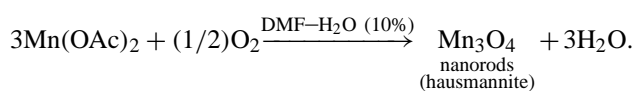
Besides, there is another hydrolysis equilibrium with the acetate anions:



Therefore, it is fair to think that the medium is basic enough to drive the formation of $\text{Mn}(\text{OH})_2$, which is later oxidized to Mn_3O_4 with simultaneous reduction of atmospheric oxygen; it is noteworthy that manganese nanoparticles are 30 times more efficient at promoting the manganese oxidation reaction than the same material in bulk [33]:



Finally, this redox process makes the hausmannite the most stable product:



4. Conclusions

We have demonstrated that simple dissolution of manganese(II) acetate in a mixture of polar solvents DMF–H₂O (10%) at room temperature can be employed to obtain Mn_3O_4 nanoparticles in one step. These nanocrystals have an elongated morphology (rodlike shape) with a preferential orientation along the $\langle 001 \rangle$ direction. The magnetic behavior is under the influence of the rod size, showing high values of remanence ratio and coercivity. It is important to note that this novel synthesis method is clean and reproducible, requires neither complex apparatus and sophisticated techniques nor templates, and can be extended to other transition metal acetates in order to obtain different metal oxides; efforts aimed at exploring this possibility are currently under investigation in our laboratory.

Acknowledgments

The support of this research by the CONACyT project J36514-E is gratefully acknowledged. We would like to thank David Morales-Morales, José Fripiat for their valuable comments and Josefina Elizalde-Torres for technical support.

References

- [1] W. Zang, Z. Yang, Y. Liu, S. Tang, X. Han, M.J. Chen, *Cryst. Growth* 263 (2004) 394.
- [2] G. Zhou, F. Rong, C. Xian-Hui, W. Yi-Cheng, *Inorg. Chem. Commun.* 4 (2001) 294.
- [3] Z. Weixin, W. Cheng, Z. Xiaoming, X. Yi, Q. Yitai, *Solid State Ionics* 117 (1999) 331.

- [4] W. Wang, C. Xu, G. Wang, Y. Liu, C. Zheng, *Adv. Mater.* 14 (2002) 837.
- [5] D. Makovec, M. Drofénik, A. Žnidarsic, *J. Eur. Ceram. Soc.* 21 (2001) 1945.
- [6] R. Ramachandran, *J. Mater. Sci.: Mater. Electron.* 13 (2003) 257.
- [7] M. Drofénik, A. Žnidaršič, M. Kristl, A. Košak, D. Makovec, *J. Mater. Sci.* 38 (2003) 3063.
- [8] S. Fritsch, J. Sarrias, A. Rousset, G.U. Kulkarni, *Mater. Res. Bull.* 33 (1998) 1185.
- [9] O.Y. Gorbenko, I.E. Graboy, V.A. Amelichev, A.A. Bosak, A.R. Kaul, B. Güttler, V.L. Svetchnikov, H.W. Zandbergen, *Solid State Commun.* 124 (2002) 15.
- [10] V. Berbenni, V. Marini, *Mater. Res. Bull.* 38 (2003) 1859.
- [11] J.M. Boyero, E.L. Fernández, J.M. Gallardo-Amores, R.C. Ruano, V.E. Sánchez, E.B. Pérez, *Int. J. Inorg. Mater.* 3 (2001) 889.
- [12] F.A. Al Sagheer, M.A. Hasan, L. Pasupulety, M.I. Kaki, *J. Mater. Sci. Lett.* 18 (1999) 209.
- [13] E.R. Stobbe, B.A. de Boer, J.W. Geus, *Catal. Today* 47 (1999) 161.
- [14] W.S. Seo, H.H. Joe, B. Kim, J.T. Park, *Angew. Chem. Int. Ed.* 43 (2004) 1115.
- [15] B. Yang, H. Hu, C. Li, X. Yang, Q. Li, Y. Qian, *Chem. Lett.* 33 (2004) 804.
- [16] A. Vázquez-Olmos, D. Díaz, G. Rodríguez-Gattorno, J.M. Saniger-Blesa, *Colloid Polym. Sci.* 282 (2004) 957.
- [17] J. Németh, G. Rodríguez-Gattorno, A.R. Vázquez-Olmos, D. Díaz, I. Dékány, *Langmuir* 20 (2004) 2855.
- [18] G. Rodríguez-Gattorno, P. Santiago-Jacinto, L. Rendon-Vázquez, J. Németh, I. Dékány, D. Díaz, *J. Phys. Chem. B* 107 (2003) 12597.
- [19] G. Rodríguez-Gattorno, D. Díaz, L. Rendón, G.O. Hernández-Segura, *J. Phys. Chem. B* 106 (2002) 2482.
- [20] R.V. Kumar, Y. Diamant, A. Gedanken, *Chem. Mater.* 12 (2000) 2301.
- [21] I. Pastoriza-Santos, L.M. Liz-Marzán, *Pure Appl. Chem.* 72 (2000) 83.
- [22] A. Bravais, *Etudes Crystallographiques*, Academie des Sciences, Paris, 1913.
- [23] J.D.H. Donnay, D. Harker, *Amer. Mineral.* 22 (1937) 463.
- [24] G. Friedel, *Bull. Soc. Fr. Mineral.* 30 (1907) 326.
- [25] V.G. Kumar, D. Aurbuch, A. Gedanken, *Ultrason. Sonochem.* 10 (2003) 17.
- [26] K. Dwight, N. Menyuk, *Phys. Rev.* 119 (1960) 1470.
- [27] C.B. Azzoni, M.C. Mozzati, L. Malavasi, P. Ghigna, G. Flor, *Solid State Commun.* 119 (2001) 591.
- [28] Y.Q. Chang, X.Y. Xu, X.H. Luo, C.P. Chen, D.P. Yu, *J. Cryst. Growth* 264 (2004) 232.
- [29] A.J. Rondinone, A.C.S. Samia, Z.J. Zhang, *J. Phys. Chem. B* 103 (1999) 6876.
- [30] J. García-Otero, M. Porto, J. Rivas, A. Bunde, *Phys. Rev. Lett.* 84 (2000) 167.
- [31] R.S. Tebble, D.J. Craik, *Magnetic Materials*, Academic Press, New York, 1969, p. 993.
- [32] R.H. Kodama, *J. Magn. Magn. Mater.* 200 (1999) 359.
- [33] M.F. Hochella, C.J. Tadanier, S.K. Lower, B.H. Lower, T.A. Kendall, T.A. Cail, A.S. Madden, *Geochim. Cosmochim. Acta* 67 (2003) A153.